An Energy Balance Model with Permafrost Feedback

Nate Nethercott

1 Permafrost

1.1 Background

Perennially frozen soils contain massive amounts of carbon, which become increasingly susceptible to thaw as global temperatures rise. Carbon released from the permafrost contributes to atmospheric green house gas (GHG) burden, which in turn accelerates the warming process and results in further carbon losses from these soils. This is permafrost feedback.

In this permafrost module we limit our analysis to carbon stored within the top three meters of High-Arctic permafrost soils, where the Arctic is defined as the region north of 60° N latitude. Carbon emission rates are determined from aerobic conditions, soil type and pool decomposition speed. We consider two soil types described by their organic carbon content (C); mineral soils which are less than 20%C by weight and organic soils that are greater than or equal to 20%C by weight (Deimling et al., 2015). We use an eight pool decomposition model where carbon falls into a passive, slow or active decomposition pool based on its lability (ease of decomposition). Carbon in the active pool is respired by permafrost soils within a year, carbon in the slow pool on a decadal scale, and carbon in the passive pool over hundreds to thousands of years (Schädel et al., 2014). We disregard the passive pool in our model.

In the simplest case, carbon is assumed to be respired from the permafrost in the form of CO_2 or CH_4. What determines this is the availability of oxygen in the decay process. It is assumed that aerobic decomposition produces strictly CO_2 while anaerobic decomposition produces CH_4. Of the carbon which decomposes anaerobically, a fraction is oxidized before reaching the surface-atmosphere interface. We assume this oxidized fraction is released as CO_2.

Both CO_2 and CH_4 are "well-mixed" within the atmosphere. The atmospheric lifetime of CH_4 is around 8.4 years due to removal by global sinks (OH radical, soil and ocean) Dentener et al., 2001. We assume the decay of CH_4 produces strictly CO_2 and has a half life of $8.4/2 = 4.2$ years.

1.2 Decomposition

Suppose carbon is distributed within the soil according to some function $m(z,t)$. Using a temperature-dependent decay rate constant, $k(T)$ (see Section 5), we express the decomposition of carbon at a specific depth in the soil as

$$\frac{dm(z,t)}{dt} = -k(T_S(z,t))m(z,t). \tag{1}$$

Let us denote by $m_O(z,t)$ the mass distribution of carbon in pools where aerobic decomposition takes place, and $m_N(z,t)$ the mass distribution of carbon in anaerobic pools. These pools decompose according to equation (13) with their own decay rate constants. We then express the general decay of permafrost carbon into CO_2 and CH_4 as follows

$$\frac{dCO_2(t)}{dt} = \frac{M_{CO_2}}{M_C}\int_{Z_L}^{0} k_O(T_S(z,t))m_O(z,t)dz, \tag{2}$$

$$\frac{dCH_4(t)}{dt} = \frac{M_{CH_4}}{M_C}\int_{Z_L}^{0} k_N(T_S(z,t))m_N(z,t)dz. \tag{3}$$

Here M_C, M_{CO_2} and M_{CH_4} are the molar masses of C, CO_2 and CH_4. Equations (14) and (15) describe release rates of each gas. One should note that since we've assumed carbon is only in the top 3 m, the lower bound on the integrals above can be replaced with -3.

Once in the atmosphere we must consider sink terms which acts to remove CH_4 and convert it to CO_2 (by assumption). Modifying the above equations we obtain

$$\frac{dCO_2(t)}{dt} = \frac{M_{CO_2}}{M_C}\int_{Z_L}^{0} k_O(T_S(z,t))m_O(z,t)dz + \left(\frac{M_{CO_2}}{M_{CH_4}}\right) r_{CH_4} CH_4(t), \tag{4}$$

$$\frac{dCH_4(t)}{dt} = \frac{M_{CH_4}}{M_C}\int_{Z_L}^{0} k_N(T_S(z,t))m_N(z,t)dz - r_{CH_4} CH_4(t), \tag{5}$$

where r_{CH_4} is the decay rate constant for the removal of CH_4.

2 EBM

The surface slab is split into two components; ocean and land. The temperature of the ocean section is assumed to be uniform both vertically and horizontally to a depth Z_O, while the temperature of the land portion changes only with depth. We make the assumption that at the surface of both mediums their temperatures are equal, i.e. $T_O \equiv T_S(0,t)$ where T_O is the temperature of the ocean and $T_S(z,t)$ represents the temperature of the soil at time t and at depth $-Z_L \leq z \leq 0$. Land and ocean areas are assumed to be "well-mixed" so that the surface slab contains ocean and land components in representative proportions.

We assume flux within the soil section to be one-dimensional, acting normal to the surface-atmosphere interface. Applying energy conservation in the ocean layer and using the heat equation to model conduction in the soil yields

$$\rho_O c_O Z_O \frac{\partial T_O(t)}{\partial t} = -K_L \frac{\partial T_S(0,t)}{\partial z} + q(0,t), \tag{6}$$

$$\rho_L c_L \frac{\partial T_S(z,t)}{\partial t} = K_L \frac{\partial^2 T_S(z,t)}{\partial z^2}, \tag{7}$$

$$T_S(-Z_L, t) = T_{Z_L}, \tag{8}$$

where ρ is density in kg m^{-3}, c is specific heat capacity in J kg^{-1} K^{-1}, Z_O is the depth of our ocean slab in m, K_L the thermal conductivity of land in W m^{-1} K^{-1}, and q is the total flux source at the surface in W m^{-2}. Note that by equation (3) we impose the boundary condition that there exists a depth where temperature remains constant in the soil.

Building on the EBM as outlined in Dortmans et al., 2019 (see README) which summarizes sources of land-atmosphere energy flux, the system of equations governing the climate model becomes

$$\begin{aligned}
\rho_A c_A Z_A \frac{dT_A(t)}{dt} &= F_A + F_C + \xi_A Q + \eta I_S - I_A, \\
\rho_O c_O Z_O \frac{\partial T_S(0,t)}{\partial t} &= -K_L \frac{\partial T_S(0,t)}{\partial z} + F_O - F_C + (1-\alpha)F_S - I_S + \beta I_A, \\
\rho_L c_L \frac{\partial T_S(z,t)}{\partial t} &= K_L \frac{\partial^2 T_S(z,t)}{\partial z^2}, \\
T_S(-Z_L, t) &= T_{Z_L}.
\end{aligned}$$

We non-dimensionalize the above system using the following dimensionless variables

$$s = \frac{\sigma T_R^4}{c_O \rho_O Z_O T_R} t, \qquad \tau_S = \frac{T_S}{T_R}, \qquad \tau_A = \frac{T_A}{T_R}, \qquad \zeta = \frac{z}{Z_L},$$

where σ is the Stefan-Boltzmann constant and $T_R = 273.15K$ is our reference temperature. Here one unit of dimensionless time s corresponds to the amount of actual time required for the earth at T_R to radiate an amount of energy equivalent to that which is stored in our ocean slab at T_R.

The non-dimensional system becomes

$$H_1 \frac{d\tau_A(s)}{ds} = f_A + f_C + \xi_A q + \eta i_S - i_A, \tag{9}$$

$$\frac{\partial \tau_S(0,s)}{\partial s} + H_2 \frac{\partial \tau_S(0,s)}{\partial \zeta} = f_O - f_C + (1-\alpha) f_S - i_S + \beta i_A, \tag{10}$$

$$H_3 \frac{\partial \tau_S(\zeta, s)}{\partial s} = \frac{\partial^2 \tau_S(\zeta, s)}{\partial \zeta^2}, \tag{11}$$

$$\tau_S(-1, s) = \tau_{Z_L}, \tag{12}$$

where

$$H_1 = \frac{\rho_A c_A Z_A}{\rho_O c_O Z_O}, \qquad H_2 = \frac{K_L}{Z_L \sigma T_R^3}, \qquad H_3 = \frac{\rho_L c_L Z_L^2 \sigma T_R^3}{K_L \rho_O c_O Z_O}, \qquad \tau_{Z_L} = \frac{T_{Z_L}}{T_R},$$
$$f_A = \frac{F_A}{\sigma T_R^4}, \qquad f_C = \frac{F_C}{\sigma T_R^4}, \qquad f_O = \frac{F_O}{\sigma T_R^4}, \qquad q = \frac{Q}{\sigma T_R^4}, \qquad i_S = \frac{I_S}{\sigma T_R^4},$$
$$i_A = \frac{I_A}{\sigma T_R^4}.$$

We are interested in equilibrium solutions to our system of equations where $\tau_S(\zeta, s) = \tau_S(\zeta)$ and $\tau_A(s) = \tau_A$. Our system thus becomes

$$0 = f_A + f_C + \xi_A q + \eta i_S - i_A, \tag{13}$$

$$H_2 \frac{\partial \tau_S(0)}{\partial \zeta} = f_O - f_C + (1-\alpha) f_S - i_S + \beta i_A, \tag{14}$$

$$0 = \frac{\partial^2 \tau_S(\zeta)}{\partial \zeta^2}, \tag{15}$$

$$\tau_S(-1) = \tau_{Z_L}. \tag{16}$$

From these equations we extract the following implicit relation,

$$\tau_S(\zeta) = \tau_{Z_L} + \frac{\zeta + 1}{H_2}[f_O - (1-\beta) f_C + (1-\alpha) f_S - (1-\beta\eta) i_S + \beta(f_A + \xi_A q)]. \tag{17}$$

3 Modelling

In the numerical model we track mass distributions in eight carbon pools, each described by a unique combination of soil type, aerobicity and decomposition speed:

- mineral aerobic fast: m_{MAF}
- mineral aerobic slow: m_{MAS}
- mineral anaerobic fast: m_{MNF}
- mineral anaerobic slow: m_{MNS}
- organic aerobic fast: m_{OAF}
- organic aerobic slow: m_{OAS}

- organic anaerobic fast: m_{ONF}
- organic anaerobic slow: m_{ONS}

For notational convenience in calculation, we will denote these pools as m_{xyw} where $x \in X = \{M, O\}$, $y \in Y = \{A, N\}$, and $w \in W = \{F, S\}$.

The initial mass of carbon in each pool (expressed as a fraction of the total estimated carbon stocks) is determined from literature. They are derived in Section 5 and shown below in Table 1

Pool	**Fraction**
m_{MAF}	8.74×10^{-3}
m_{MAS}	7.20×10^{-2}
m_{MNF}	4.60×10^{-4}
m_{MNS}	3.79×10^{-3}
m_{OAF}	8.76×10^{-4}
m_{OAS}	1.71×10^{-2}
m_{ONF}	3.50×10^{-3}
m_{ONS}	6.84×10^{-2}

Table 1: Initial fractions of total estimated carbon in each pool

When summing contributions of each pool we find that only 17.5% of the total carbon in the top three meters is available for thaw. The rest of the carbon is inert (i.e. it is characterized by passive decomposition).

We construct discrete mass distribution functions for each pool by partitioning the top three meters of our surface slab into P levels. Denote by $m^i(t) = m(z^i, t)$ the mass distribution of carbon in level i with $z^i = -3(\frac{i-0.5}{P})$. Likewise, define by $T^i(t) = T(z^i, t)$ the temperature of the ith level. The initial carbon distribution is uniform across P levels in each pool at $t = t_0$.

We then describe the evolution of the carbon distribution in the soil according to

$$\frac{dm^i(t)}{dt} = \sum_{x \in X} \sum_{y \in Y} \sum_{w \in W} -k(\kappa_{xyw}, T^i(t)) m^i_{xyw}(t). \tag{18}$$

Here $k(\kappa, T_S(z,t))$ is an annual effective decomposition rate given generally by

$$k(\kappa, T_S(z,t)) = \frac{1}{2\pi} \int_0^{2\pi} \kappa \cdot g(T,t) dt, \tag{19}$$

where

$$g(T,t) = \begin{cases} Q_{10}^{\frac{T + \Delta T \sin t - T_{ref}}{10}} & T + \Delta T \sin t > 0, \\ 0 & \text{otherwise.} \end{cases} \tag{20}$$

Using assumptions outlined in Section 1, as well as factors listed in Table 3, we express CO_2 emissions as a sum of aerobic and anaerobic + oxidation processes

$$\begin{aligned}\frac{dCO_2(t)}{dt} &= \frac{M_{CO_2}}{M_C}\sum_{i=1}^{P}\sum_{x\in X}\sum_{w\in W} k(\kappa_{xAw}, T^i(t))m^i_{xAw}(t) \\ &+ \frac{M_{CO_2}}{M_C}\sum_{i=1}^{P}\sum_{x\in X}\sum_{w\in W} k(R\kappa_{xAw}, T^i(t))m^i_{xNw}(t)\cdot\chi_x,\end{aligned} \tag{21}$$

or equivalently

$$\frac{dCO_2(t)}{dt} = \frac{M_{CO_2}}{M_C}\sum_{i=1}^{P}\sum_{x\in X}\sum_{w\in W} k(\kappa_{xAw}, T^i(t))[m^i_{xAw}(t) + Rm^i_{xNw}(t)\cdot\chi_x].$$

CH_4 emissions are then described by

$$\frac{dCH_4(t)}{dt} = \frac{M_{CH_4}}{M_C}\sum_{i=1}^{P}\sum_{x\in X}\sum_{w\in W} k(R\kappa_{xAw}, T^i(t))m^i_{xNw}(t)\cdot(1-\chi_x). \tag{22}$$

Finally, taking into account the removal of CH_4 within the atmosphere, our governing equations become

$$\begin{aligned}\frac{dm^i(t)}{dt} &= \sum_{x\in X}\sum_{w\in W} -k(\kappa_{xyw}, T^i(t))[m^i_{xAw}(t) + Rm^i_{xNw}(t)], \\ \frac{dCO_2(t)}{dt} &= \frac{M_{CO_2}}{M_C}\sum_{i=1}^{P}\sum_{x\in X}\sum_{w\in W} k(\kappa_{xAw}, T^i(t))[m^i_{xAw}(t) + Rm^i_{xNw}(t)\cdot\chi_x] \\ &+ \frac{M_{CO_2}}{M_{CH_4}} r_{CH_4} CH_4(t), \\ \frac{dCH_4(t)}{dt} &= \frac{M_{CH_4}}{M_C}\sum_{i=1}^{P}\sum_{x\in X}\sum_{w\in W} k(R\kappa_{xAw}, T^i(t))m^i_{xNw}(t)\cdot(1-\chi_x) - r_{CH_4}CH_4(t).\end{aligned} \tag{23}$$

The solution to this system of P+2 differential equations is a function $u(t)$ such that

$$\dot{u(t)} = \begin{bmatrix} \frac{m^1(t)}{dt} \\ \frac{m^2(t)}{dt} \\ \vdots \\ \frac{m^P(t)}{dt} \\ \frac{dCO_2(t)}{dt} \\ \frac{dCH_4(t)}{dt} \end{bmatrix},\ u(t_0) = \begin{bmatrix} m^1(t_0) \\ m^2(t_0) \\ \vdots \\ m^P(t_0) \\ 0 \\ 0 \end{bmatrix}.$$

Here we assume that no permafrost carbon is present in the atmosphere in the year t_0. We numerically solve for $u(t)$ using a Adams-Bashforth 3-step method along different representative concentration pathways (RCPs) with $u(t_1)$ and $u(t_2)$ being obtained from a third order Runge-Kutta method.

4 Results

When considering the impact of including permafrost terms in a climate model, the natural assumption is that the onset of a bifurcation (if any) will be advanced. In the very least we assume additional carbon burdens introduced by permafrost thaw will result in proportionally warmer Arctic surface temperatures. It would be nice if numerical analysis validated our intuition.

Using RCP projections and their extensions (ECPs) in tandem with historical records we are able to prescribe realistic non-permafrost sourced carbon and methane concentrations on an annual basis from 1765 until 2500. We will limit our simulations to the range of years between 1900 and 2300 inclusive.

When plotting the permafrost and no-permafrost situations we see our initial supposition is supported. In Fig.1 we find that the inclusion of permafrost terms results in a bifurcation along RCP 8.5 in the year 2115 whereas this occurs without permafrost considerations four years later in 2119.

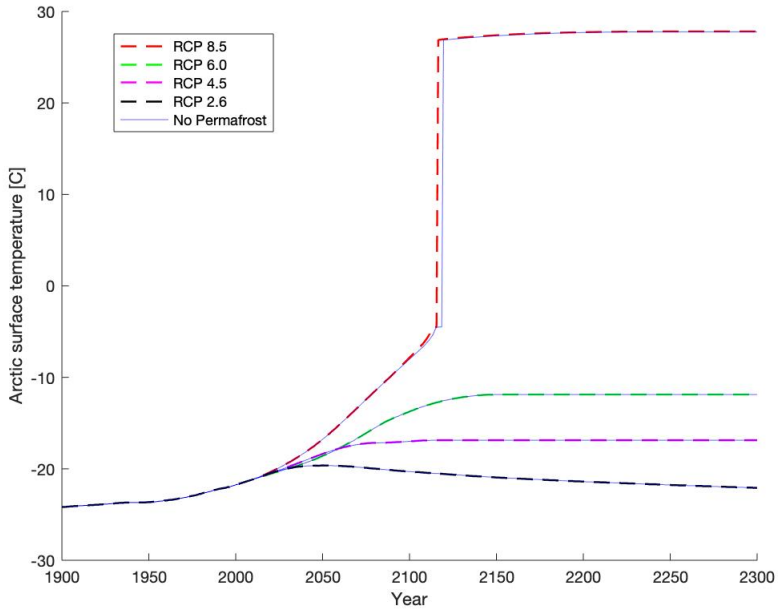

Figure 1: Arctic surface temperatures simulated along the four RCP pathways from 1900 to 2300 while considering permafrost feedback.

At the point of bifurcation, 101.8 PgC has been released. By the end of our simulation in the year 2300, this value has risen to 191.6 PgC. This estimate falls inside the range of values outlined in Mcguire et al., 2018 who report 641 PgC losses to 167 PgC gains on either extreme by the year 2300. At the end of simulation, the net mass of CH_4 is only 1.43 TgC. CO_2 and CH_4 emissions from the permafrost along RCP 8.5 had the effect of increasing global levels by 53.3 ppm and 814.4 ppb respectively.

In Fig. 1 we've prescribed the EBM with intermediate Arctic atmospheric and ocean heat fluxes of $F_A = 104$ W m^{-2} and $F_O = 10$ W m^{-2} respectively. We find that, as illustrated in Fig.2, almost no characteristic change is observed when instead running our simulation using a linear interpolation of flux values as reported by Koenigk and Brodeau, 2014 (Table 2). The only thing worth noting here is the observable divergence of RCP 6.0 from the no-permafrost baseline.

Table 2: Atmosphere and ocean heat fluxes into the Arctic as simulated in Koenigk and Brodeau, 2014, using the global coupled climate model EC-Earth. We take linearly interpolate between RCPs 8.5 and 2.6 to construct appropriate projections for RCPs 4.5 and 6.0.

Year	**Scenario**	F_A **(W m^{-2})**	F_O **(W m^{-2})**
1850	Historical	107.28	9.75
2100	RCP 2.6	104.03	13.00
2100	RCP 8.5	97.53	19.5

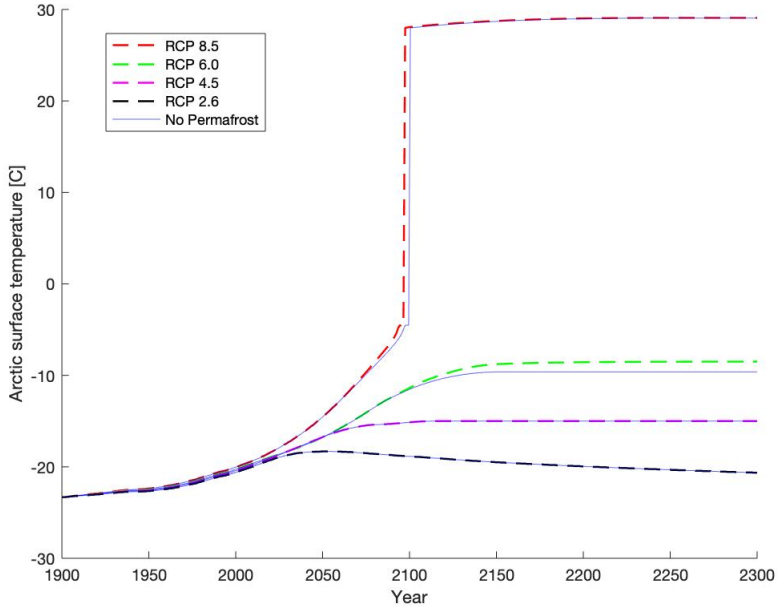

Figure 2: Arctic surface temperatures simulated along RCPs from 1900 to 2300 using Koenigk and Brodeau, 2014 flux data. F_A and F_O change linearly with values in the years 1850 and 2100 as described by Table 1. Appropriate heat flux "pathways" for RCPs 4.5 and 6.0 were obtained through simple interpolation. After 2100 these fluxes are held constant until the year 2300.

When simulating the EBM using instead F_A projections obtained from Yang et al., 2016 we find that a bifurcation results along RCP 6.0 regardless of the inclusion of permafrost feedback, see Fig. 3. In this scenario F_A reaches a peak value of 129 W m^{-2} in 2100 after which it is held constant. Note also that a bifurcation takes place along RCP 4.5 when one considers permafrost feedback.

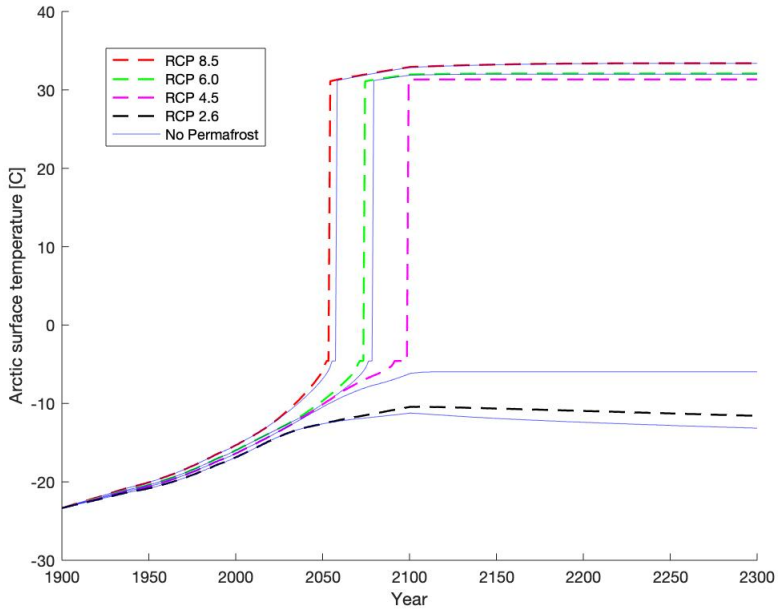

Figure 3: Arctic surface temperatures simulated along RCPs from 1900 to 2300 using Yang et al., 2016 F_A data. F_O is as before, and both fluxes increase linearly until 2100 after which they are held constant.

All in all, the effects of permafrost feedback on the EBM, though noticeable, are not significant. Without modifying other forcing parameters, simulations run with and without permafrost feedback were characteristically similar. The bifurcation along RCP 8.5 was only advanced by four years, and no new bifurcations were produced in the mitigation scenarios.

Limitations in the model include the use of steady state methods for the heat equation, the assumption of a uniform material for the surface slab, no latent heat effects, flux in 1-D, and a ocean slab without a temperature gradient. We also do not model net primary productivity (NPP) and other plant effects which might function to offset losses from emissions.

5 Supplementary

5.1 Physical parameters

Symbol	Description	Value	Reference
C_{tot}	Total C stocks	1095 PgC	Hugelius et al., 2014
S_A	Surface area of Arctic region	3.42×10^{13} m^2	N/A
S_P	Permafrost surface area	1.78×10^{13} m^2	Hugelius et al., 2014
Z_L	Soil slab depth	15 m	Biskaborn et al., 2018
$T_S(Z_L, t)$	Constant temperature at bottom of surface slab	-3.054°C	Biskaborn et al., 2018
K_L	Thermal conductivity of land	2 W m^{-1} K^{-1}	**SOURCE**
$\gamma_{a,m}$	Initial fraction of carbon available for decomposition in active pool, mineral soils	0.013	Schädel et al., 2014
$\gamma_{s,m}$	Initial fraction of carbon available for decomposition in slow pool, mineral soils	0.107	Schädel et al., 2014
$\gamma_{a,o}$	Initial fraction of carbon available for decomposition in active pool, organic soils	0.015	Schädel et al., 2014
$\gamma_{s,o}$	Initial fraction of carbon available for decomposition in slow pool, organic soils	0.293	Schädel et al., 2014
f_m	Initial mass fraction of carbon in mineral soils	0.708	Hugelius et al., 2014
f_o	Initial mass fraction of carbon in organic soils	0.292	Hugelius et al., 2014
$A_{m,n}$	Initial area fraction of mineral soil with anaerobic decomposition	0.05	Deimling et al., 2012
$A_{o,n}$	Initial area fraction of organic soils with anaerobic decomposition	0.8	Frolking et al., 2001
χ_m	Oxidation constant in mineral soils	0.25	Deimling et al., 2012
χ_o	Oxidation constant in organic soils	0.6	Deimling et al., 2012
R	Ratio of decomposition rates in aerobic and anaerobic conditions	0.1	Deimling et al., 2012
Q_{10}	Q_{10} temperature sensitivity	2.5	Schädel et al., 2014
$\kappa_{a,m}$	Active pool decomposition rate constant at 5 °C in mineral soils under aerobic conditions	2.8986	Schädel et al., 2014
$\kappa_{s,m}$	Slow pool decomposition rate constant at 5 °C in mineral soils under aerobic conditions	0.1318	Schädel et al., 2014

$\kappa_{a,o}$	Active pool decomposition rate constant at 5 °C in organic soils under aerobic conditions	2.4390	Schädel et al., 2014
$\kappa_{s,o}$	Slow pool decomposition rate constant at 5 °C in organic soils under aerobic conditions	0.1387	Schädel et al., 2014
r_{CH_4}	Atmospheric decay rate of CH_4	0.165	**SOURCE**

Table 3: Constants used in permafrost module

5.2 Initial mass of carbon

A simple application of the factors listed in the table above shows that at $t = t_0$, the mass of carbon in each of the 8 pools is given by

$$C_{MAF} = C_{tot} \cdot f_m(1 - A_{m,an})\gamma_{a,m} = C_{tot} \cdot 8.74 \times 10^{-3} = 9.57\, PgC, \quad (24)$$

$$C_{MAS} = C_{tot} \cdot f_m(1 - A_{m,an})\gamma_{s,m} = C_{tot} \cdot 7.20 \times 10^{-2} = 78.84\, PgC, \quad (25)$$

$$C_{MNF} = C_{tot} \cdot f_m A_{m,an}\gamma_{a,m} = C_{tot} \cdot 4.60 \times 10^{-4} = 0.50\, PgC, \quad (26)$$

$$C_{MNS} = C_{tot} \cdot f_m A_{m,an}\gamma_{s,m} = C_{tot} \cdot 3.79 \times 10^{-3} = 4.15\, PgC, \quad (27)$$

$$C_{OAF} = C_{tot} \cdot f_o(1 - A_{o,an})\gamma_{a,o} = C_{tot} \cdot 8.76 \times 10^{-4} = 0.96\, PgC, \quad (28)$$

$$C_{OAS} = C_{tot} \cdot f_o(1 - A_{o,an})\gamma_{s,o} = C_{tot} \cdot 1.71 \times 10^{-2} = 18.72\, PgC, \quad (29)$$

$$C_{ONF} = C_{tot} \cdot f_o A_{o,an}\gamma_{a,o} = C_{tot} \cdot 3.50 \times 10^{-3} = 3.83\, PgC, \quad (30)$$

$$C_{ONS} = C_{tot} \cdot f_m A_{o,an}\gamma_{s,o} = C_{tot} \cdot 6.84 \times 10^{-2} = 74.89\, PgC. \quad (31)$$

5.3 Absorptivity CH_4

In Schmidt et al., 2010 we see that the authors attribute 50% of the modern day absorption factor to water vapour, 25% to clouds, 19% to CO_2 and 7% to other gasses. Of the other gasses, CH_4 accounts for 1 seventh of the absorption, so CH_4 contributes 1% overall. We will lump the remaining effects into the fraction for CO_2. The modern-day value for η is 0.9, so

$$0.9 = 1 - (1 - 50x)(1 - 25x)(1 - 24x)(1 - x). \quad (32)$$

Solving the quartic for x yields $x = 0.01494$. We also have that

$$x = 1 - e^{-\nu \cdot \frac{M_{CH_4}}{M} \times 10^{-9} k_M \frac{P_A}{g}}. \quad (33)$$

Taking the molar mass of methane to be 16.04 g mol^{-1}, the molar mass of atmosphere to be 28.97 g mol^{-1} (so $mmCH_4/mmAtm = 0.554$) and year 2000 levels of CH_4 to be 1751 ppb, we solve for k_M as follows

$$k_M = \frac{-g \ln(1 - x)}{0.554 \cdot \nu \times 10^{-9} P_A} = 1.4968. \quad (34)$$

We then calculate G_M as follows:

$$G_M = 0.554 \times 10^{-9} k_M \frac{P_A}{g} = 8.5410 \times 10^{-6}. \tag{35}$$

5.4 Insolation

From McGehee, 2012 the latitude-dependence of insolation is given by the relation,

$$insolation = Qs(y), \tag{36}$$

where Q is the global annual average insolation and $y = sin(\varphi)$ with φ representing latitude. $s(y)$ is a distribution of relative insolation coefficients given by

$$s(y) = \frac{2}{\pi^2} \int_0^{2\pi} \sqrt{1 - (\sqrt{1-y^2}\sin\beta\cos\gamma - y\cos\beta)^2} d\gamma, \tag{37}$$

$$\int_0^1 s(y)dy = 1, \tag{38}$$

where β is the obliquity (here taken as $\beta = 23.5°$) and γ is the longitude.

Taking the globally averaged solar radiation as $Q = 340$ W m^{-2} and realizing that $y = sin(\varphi) \implies dy = cos(\varphi)d\varphi$, we compute the average insolation over the Arctic region (A) defined as any region with latitude $\geq 60°$as

$$\begin{aligned} Q_A &= Q \cdot \frac{\int_A s(y)dy}{\int_A dy} \\ &= Q \cdot \frac{\int_{\frac{\pi}{3}}^{\frac{\pi}{2}} \frac{2}{\pi^2} \int_0^{2\pi} \sqrt{1 - (\sqrt{1-(\sin\varphi)^2}\sin\beta\cos\gamma - \sin\varphi\cos\beta)^2} d\gamma \cdot \cos(\varphi)d\varphi}{\int_{\frac{\pi}{3}}^{\frac{\pi}{2}} \cos(\varphi)d\varphi} \\ &\approx 201.73\, W\, m^{-2}. \end{aligned}$$

5.5 Convert between mass rate and concentration rate

Given the left-hand sides of equations (4) and (5) we wish to translate the emission rates from units of Pg C a^{-1} to units of ppm(ppb) a^{-1}.

First we calculate the volume of the atmosphere as defined within the context of the EBM as follows:

$$V = 2 \int_0^{2\pi} \int_0^{\frac{\pi}{2}} \int_{r_E}^{r(\varphi)} \rho^2 \sin\varphi d\rho d\varphi d\theta. \tag{39}$$

Here r_E is the radius of the Earth and $r(\varphi)$ is a function describing troposphere height as a function of polar angle. The radius function takes the values of r_E

+ 9000 km at $\varphi = 0$ and r_E + 14000 km at $\varphi = \frac{\pi}{2}$ which is consistent with the original EBM described in Dortmans et al., 2019. A linear model for this is

$$r(\varphi) = (\frac{5000}{\frac{\pi}{2}})\varphi + 9000 + r_E. \tag{40}$$

Emission rates are then expressed in molar ratios ($\dot{\mu}$, $\dot{\nu}$) as

$$\dot{\mu} = \frac{1}{\rho_A V}\frac{M_A}{M_{CO_2}}\frac{dCO_2}{dt}, \tag{41}$$

$$\dot{\nu} = \frac{1}{\rho_A V}\frac{M_A}{M_{CH_4}}\frac{dCH_4}{dt}, \tag{42}$$

where ρ_A is atmospheric density in kg m^{-3}, and M_x a molar mass in kg mol^{-1}.

References

Biskaborn, B. K., Smith, S. L., Noetzli, J., Matthes, H., Vieira, G., Streletskiy, D. A., Schoeneich, P., Romanovsky, V. E., Lewkowicz, A. G., Abramov, A., Allard, M., Boike, J., Cable, W. L., Christiansen, H. H., Delaloye, R., Diekmann, B., Drozdov, D. S., Etzelmüller, B., Grosse, G., ... Lantuit, H. (2018). *GTN-P global mean annual ground temperature data for permafrost near the depth of zero annual amplitude (2007-2016)* (tech. rep.). https://doi.org/10.1038/s41467-018-08240-4

Deimling, T. S. V., Grosse, G., Strauss, J., Schirrmeister, L., Morgenstern, A., Schaphoff, S., Meinshausen, M., & Boike, J. (2015). Observation-based modelling of permafrost carbon fluxes with accounting for deep carbon deposits and thermokarst activity. *Biogeosciences*, *12*, 3469.

Deimling, T. S. V., Meinshausen, M., Levermann, A., Huber, V., Frieler, K., Lawrence, D., & Brovkin, V. (2012). Estimating the near-surface permafrost-carbon feedback on global warming. *Biogeosciences*, *9*, 649.

Dentener, F., Derwent, R., Dlugokencky, E., Holland, E., Isaksen, I., Katima, J., Kirchhoff, V., Matson, P., Midgley, P., & Wang, M. (2001). *Climate change 2001: The scientific basis. contribution of working group i to the third assessment report of the intergovernmental panel on climate change[[houghton, j.t., y. ding, d.j. griggs, m. noguer, p.j. van der linden, x. dai, k. maskell, and c.a. johnson (eds.)]* (tech. rep.). IPCC.

Dortmans, B., Langford, W. F., & Willms, A. R. (2019). An energy balance model for paleoclimate transitions. *Climate of the Past*, *15*(2), 493–520. https://doi.org/10.5194/cp-15-493-2019

Frolking, S., Roulet, N. T., Moore, T. R., Richard, P. J. H., Lavoie, M., & Muller, S. D. (2001). Modeling Northern Peatland Decomposition and Peat Accumulation. *Ecosystems*, *4*, 479–498.

Hugelius, G., Strauss, J., Zubrzycki, S., Harden, J., Schuur, E. A. G., Ping, C.-L., Schirrmeister, L., Grosse, G., Michaelson, G., Koven, C., O'Donnell, J., Elberling, B., Mishra, U., Camill, P., Yu, Z., Palmtag, J., & Kuhry, P. (2014). Estimated stocks of circumpolar permafrost carbon with quantified uncertainty ranges and identified data gaps. *Biogeosciences*, *11*, 6573.

Koenigk, T., & Brodeau, L. (2014). Ocean heat transport into the Arctic in the twentieth and twenty-first century in EC-Earth. *Clim. Dy- nam*, *42*, 3101–3120.

McGehee, C., Richard ; Lehman. (2012). A Paleoclimate Model of Ice-Albedo Feedback Forced by Variations in Earth's Orbit. *SIAM journal on applied dynamical systems*, *11*.

Mcguire, A. D., Lawrence, D. M., Koven, C., Clein, J. S., Burke, E., Chen, G., Jafarov, E., Macdougall, A. H., Marchenko, S., Nicolsky, D., Peng, S., Rinke, A., Ciais, P., Gouttevin, I., Hayes, D. J., Ji, D., Krinner, G., Moore, J. C., Romanovsky, V., ... Mcguire, A. D. (2018). Dependence of the evolution of carbon dynamics in the northern permafrost region on the trajectory of climate change. *Proceedings of the National Academy of Sciences of the United States of America*, *115*, 3882–3887.

Schädel, C., Schuur, E. A. G., Bracho, R., Elberling, B., Knoblauch, C., Lee, H., Luo, Y., Shaver, G. R., & Turetsky, M. R. (2014). Circumpolar assessment of permafrost C quality and its vulnerability over time using long-term incubation data. *Global Change Biology*, *20*, 641–652.

Schmidt, G. A., Ruedy, R. A., Miller, R. L., & Lacis, A. A. (2010). Attribution of the present-day total greenhouse effect. *Journal of Geophysical Research: Atmospheres*, *115*.

Yang, H., Zhao, Y.-Y., & Liu, Z.-Y. (2016). Understanding Bjerknes com- pensation in atmosphere and ocean transports using a coupled box model. *Journal of Climate*, *29*, 2145–2160.